JOURNAL OF COMPUTATIONAL PHYSICS 75, 217–235 (1988)

A Spectral Collocation Method for Two-Dimensional Compressible Convection

SERGE GAUTHIER

Centre D'Études de Limeil-Valenton, B.P. 27, 94190 Villeneuve-St-Georges, France

Received July 15, 1986; revised April 30, 1987

A Fourier–Chebyshev spectral simulation of two-dimensional compressible convection is presented. The fluid is a perfect gas with constant dynamic viscosity and thermal conductivity. Both slippery and rigid boundary conditions for the velocity are used here. The temperature is maintained fixed at the upper and lower boundaries. An explicit Adams–Bashforth predictor-corrector numerical scheme is used in order to overcome the Courant–Friedriechs–Lewy condition. The nonlinear diffusion terms are handled by an iterative method, with finite differences or spectral preconditioning. Steady state solutions have been obtained for both types of boundary conditions. Critical exponents are found to be the same as in the incompressible case, at least for a weak value of the stratification parameter.

1. INTRODUCTION

In the past ten years spectral methods have brought extensive progress in the understanding of the transition to turbulence. Such insights have been possible due to the high accuracy of the spectral methods. The main properties of these methods are well documented in Refs. [1–3]. Among these properties recall the absence of phase error. Moreover, the convergence is generally faster than algebraic in the mesh size. Both properties make these methods well suited to the study of the transition to turbulence. A paradigm in this area is the incompressible thermal convection problem, studied within the framework of the Boussinesq approximation. This approximation also holds for a compressible fluid provided that the vertical extent of the fluid is small enough. In some situations, for example, stellar convection or laser driven fusion, the stratification of the fluid can no longer be ignored. Another model is then used, namely, the anelastic approximation where the density varies in space and time but not on the acoustic time scale. In other words, this approximation consists in filtering out the high frequency acoustic waves. Several studies have been carried out within this approximation [4–6], which requires that the fluid velocity is small compared to the local sound speed [7]. If this requirement is not satisfied we have to use the full Navier–Stokes equations. Such a program was first carried out by Graham [8]. Later, Chan, Sofia, and Wolff [9], using a finite differences code and an eddy viscosity for modelling the small scales of the turbulence, exhibited the breaking of the rolls at high Rayleigh numbers. This

0021-9991/88 $3.00

justified an early assumption taken in the mixing length theory of stellar convection. More recently, Hurlburt, Toomre, and Massaguer [10], using an improved version of the Graham's code, showed that there is no tendency to form multiple rolls, at least for this range of Rayleigh numbers but they did exhibit time-dependent solutions for high Rayleigh numbers. However, the subgrid-scale model used in Ref. [9] could explain the disagreement between both results.

In this paper, we present a spectral collocation method for two-dimensional compressible convection. A Fourier expansion has been used in the horizontal direction. In the inhomogeneous direction we use an expansion on the Chebyshev polynomials because of their high rate of convergence and their ability to handle sophisticated boundary conditions.

When using Chebyshev polynomials in compressible flows, we are faced with two very severe restrictions on the time step, both of which come from the high resolution on the boundaries. The first one is the Courant–Friedriechs–Lewy condition (CFL) which is worse in compressible flows due to the high frequency acoustic waves. The second one is the stability condition for the diffusion terms. Both difficulties have to be solved by an implicit or semi-implicit scheme. However, in compressible flows, viscous and thermal diffusion terms are nonlinear. This nonlinearity leads to the use of iterative methods such as suggested by Orszag [11].

We describe the physical problem in the Section 2. Section 3 is devoted to the numerical method used to solve the equations. In Section 4 we present preliminary results about steady states close to the threshold where critical exponents are computed.

2. The Physical Problem and the Equations of the Model

The motion takes place in a two-dimensional rectangular cavity of width L_x and height d. The z-axis is directed downward so that the gravity, represented by the vector $g = (0, 0, g)$, is positive along this direction.

The equations of motion for a compressible, viscous, thermally conducting gas are as follows:

$$\partial\rho/\partial t + \partial\rho\, u_i/\partial x_i = 0, \tag{2.1}$$

$$\partial\rho\, u_i/\partial t + \partial\rho\, u_i/u_j/\partial x_j = -\partial P/\partial x_i + \partial\tau_{ij}/\partial x_j + g_i\rho, \tag{2.2}$$

and

$$\partial\rho\, E/\partial t + \partial(\rho E + P)\, u_j/\partial x_j = \partial\tau_{ij}\, u_i/\partial x_j + \partial/\partial x_i\, K\, \partial T/\partial x_i, \tag{2.3}$$

where E is the total energy

$$E = \tfrac{1}{2}(u_1^2 + u_2^2) + e - gx_2, \tag{2.4}$$

and τ_{ij} is the viscous stress tensor given by

$$\tau_{ij} = \mu(\partial u_i/\partial x_j + \partial u_j/\partial x_i - \tfrac{2}{3}\delta_{ij}\,\partial u_l/\partial x_l), \tag{2.5}$$

where $i, j, l = 1, 2$. The Stokes' relation has been used between the first and the second viscosities. The coordinates x_1 and x_2 stand for the x and z coordinates, respectively.

This set of equations is closed by the equation of state for the perfect gas.

$$P = R_* \rho T \qquad \text{and} \qquad e = C_v T. \tag{2.5}$$

P, ρ, T, and e are pressure, density, temperature, and internal energy, respectively; the u_i are the components of the velocity. The thermal conductivity and the dynamic viscosity are taken as constants. R_* is the gas constant and C_v the specific heat at constant volume.

The boundary conditions have to be chosen according to the physical problem. In Hydrodynamics one usually deals with viscous fluids confined between two rigid plates. One naturally chooses rigid boundary conditions where the velocity vanishes on the walls. On the other hand, in astrophysics one is concerned with stellar convection zones, thus it is reasonable to use slippery boundary conditions where the horizontal gradient of the velocity vanishes [12]. The boundary conditions for the temperature are given by fixed temperatures at the bottom and the top of the layer. Equally we can just give the heat flux at one of these boundaries. In this paper, we will be dealing both with rigid and slippery boundary conditions for the velocity and the prescribed temperatures at the upper and lower bounds of the layer. Then, the boundary conditions read

$$u_2 = 0 \qquad \text{at } z = z_0, z_0 + d, \tag{2.6}$$

$$u_1 = 0 \qquad \text{or} \qquad \partial u_1/\partial z = 0 \qquad \text{at } z = z_0, z_0 + d, \tag{2.7}$$

$$T(z_0) = T_0 \qquad \text{and} \qquad T(z_0 + d) = T_1. \tag{2.8}$$

Periodic boundary conditions are used in the horizontal direction for all variables.

The static state is obtained by setting $\partial/\partial t = 0$ and $u_i = 0$ in Eqs. (2.1)–(2.3). This solution is a polytrope written as in Ref. [12],

$$T(z) = zZ, \tag{2.9}$$

$$\rho(z) = z^m Z^m, \tag{2.10}$$

$$P(z) = z^{m+1} Z^{m+1}, \tag{2.11}$$

The coordinate z goes from Z^{-1} to $Z^{-1} + 1$, where $Z = d/z_0$. The index of the polytrope is

$$m = g/R_* \beta_0 - 1, \qquad \text{where } \beta_0 = T(z_0 + d) - T(z_0). \tag{2.12}$$

In Eqs. (2.9)–(2.11) and henceforth, we will be using the following units: d,

$d^2\rho(z_0)/\mu$, $\rho(z_0)$, and $T(z_0)$ for length, time, density, and temperature, respectively. The two-dimensional compressible convection problem is characterized by six dimensionless parameters which are the aspect ratio A, the Prandtl number σ, the ratio of specific heats γ, the normalized layer thickness Z, the polytropic index m, and the Rayleigh number R. The parameters σ and γ are given by the thermodynamical properties of the fluid. Z characterizes the stratification of the configuration while the Rayleigh number measures the degree of the instability. Their expressions are

$$A = L_x/d, \qquad \sigma = C_p\mu/K, \qquad Z = d/z_0, \qquad \gamma = C_p/C_v,$$

and

$$R = (g/T_u)\, d^4[(T_1 - T_u)/d - g/C_p]/(K/\rho_u C_p)(\mu/\rho_u), \tag{2.13}$$

where the subscripts l and u refer to the lower and upper layer boundaries. The definition of all parameters follows the Refs [8–10, 12].

Now the set of Equations (2.1)–(2.3) can be rewritten as

$$\partial\rho'/\partial t + \partial\rho\, u_i/\partial x_i = 0, \tag{2.14}$$

$$\partial\rho\, u_i/\partial t + \partial\rho\, u_i u_j/\partial x_j = -S\partial(P+p)/\partial x_i + \partial\tau_{ij}/\partial x_j + G\rho', \tag{2.15}$$

and

$$\partial\rho\, E/\partial t + \partial(\rho E + \mathscr{P}P)\, u_j/\partial x_j = +\partial\tau_{ij}u_i/\partial x_j + S/(\gamma-1)\,\gamma/\sigma\,\partial^2\Theta/\partial x_i\,\partial x_i, \tag{2.16}$$

where ρ', Θ, and p are the density, temperature, and pressure fluctuations. S and G are auxiliary constants defined by

$$S = R/[\sigma(m+1)^2 Z^2(1/(m+1) - (\gamma-1)/\gamma] \qquad \text{and} \qquad G = ZS(m+1). \tag{2.17}$$

Four different time scales are present in this model of thermal compressible convection. Two of them are given by the first and the second viscosity. In dimensionless variables they read

$$t^1_{\text{viscous}} \sim \rho(z), \qquad t^2_{\text{viscous}} \sim 3\rho(z). \tag{2.18}$$

The time scale of the diffusion is given by

$$t_{\text{thermal}} \sim \sigma/\gamma\rho(z), \tag{2.19}$$

where the density goes from Z^m to $(Z+1)^m$. The compressibility of the model leads to high frequency acoustic waves for which the time scale is given by

$$t_{\text{acoustic}} \sim 1/(\gamma G T(z))^{1/2}, \tag{2.20}$$

where the mean temperature varies from Z to $Z+1$.

This time scale is generally smaller than the viscous time scales by two or three orders of magnitude, but according to Eq. (2.19), the thermal time scale may be of the same order of magnitude, or much smaller than the acoustic time scale. Following this remark, a large number of time steps will be needed to obtain solutions due to the necessity of resolving the smallest time scale. This has to be taken into account when building a numerical scheme, in order to lead to a reasonable computation time. Finally, we recall that the sound velocity is $c_s^2 = (\partial P/\partial \rho)_s = \gamma(\partial P/\partial \rho)_T$, or in our system of units $c_s^2 = \gamma S(\partial P/\partial \rho)_T$, where S is given by (2.17).

3. The Computational Technique

3.1. *General Formulation*

All variables are expanded in a Fourier–Chebyshev basis as

$$u(x, z, t) = \sum_{l=-N/2}^{l=N/2} \sum_{m=0}^{M} u_{lm}(t)\, e^{2\pi i l x / L_x} T_m(2z), \tag{3.1}$$

where T_m is the Chebyshev polynomial of degree m and L_x is the horizontal periodicity.

We use a collocation method where spatial derivatives are computed in the spectral space and nonlinear products are performed in the physical space on the grid points

$$x_i = iL_x/N, \qquad i = 0, 1, \ldots, N-1 \tag{3.2}$$

$$z_j = Z^{-1} + 1/2[1 + \cos(\pi(M-j)/M)], \qquad j = 0, 1, \ldots, M. \tag{3.3}$$

The evolution in time is carried out in the physical space by means of a finite differences technique.

The incompressible case is generally handled by the classic Adams–Bashforth–Crank–Nicholson (ABCN) time stepping scheme [13–15], despite its low order in time, typically of order Δt. As already stated, in compressible flows, the time step required for the convective stability, via the CFL condition is much smaller than that required for accurate resolution. This suggests that one may try to overcome this constraint by an appropriate algorithm. But a full implicit scheme would be too cumbersome, so, we have chosen a predictor-corrector technique. Our ambition, although beyond this paper, is to simulate the transition to turbulence, which requires high time resolution [1]. Thus we are aware that we probably would have to use the Richardson extrapolation method as in [16], to obtain a higher order approximation. Convection and pressure terms are treated by a second-order Adams–Bashforth predictor and a third-order Adams–Bashforth corrector [17].

Such a combination is stable for a time step of the order of the CFL condition [18]. This scheme reads

$$\begin{aligned}(\rho^* - \rho^n)/\Delta t &= -1/2(3\,\partial\rho^n\, u_i^n/\partial x_i - \partial\rho^{n-1} u_i^{n-1}/\partial x_i)\\ (\rho^{n+1} - \rho^n)/\Delta t &= -1/12(-\partial\rho^{n-1}\, u_i^{n-1}/\partial x_i + 8\,\partial\rho^n\, u_i^n/\partial x_i + 5\,\partial\rho^*\, u_i^*/\partial x_i)\end{aligned} \tag{3.4}$$

$$\begin{aligned}(u_i^* - u_i^n)/\Delta t &= -1/2(3C_i^n - C_i^{n-1})\\ (u_i^{n+1} - u_i^n)/\Delta t &= -1/12(-C_i^n + 8C_i^{n-1} + 5C_i^*)\\ &\quad + (1 + \delta_{i1}/3)\, 1/\rho\, \partial^2 u_i^{n+1}/\partial x_2^2\end{aligned} \tag{3.5}$$

with

$$\begin{aligned}C_i &= -u_j\,\partial u_i/\partial x_j - 1/\rho\, S\,\partial p/\partial x_i + (1 + \delta_{i2}/3)\, 1/\rho\,\partial u_i/\partial x_1^2\\ &\quad + 1/3\rho\,\partial^2(u_1\delta_{i2} + u_2\delta_{i1})/\partial x_1\,\partial x_2 + G\rho^1/\rho\delta_{i2}\\ (\mathscr{E}^* - \mathscr{E}^n)/\Delta t &= -1/2(3D_i^n - D_i^{n-1})\\ (\mathscr{E}^{n+1} - \mathscr{E}^n)/\Delta t &= -1/12(-D^n + 8D^{n-1} + 5D^*)\\ &\quad + S/(\gamma - 1)\,\gamma/\sigma\,\partial^2\Theta^{n+1}/\partial x_2^2\end{aligned} \tag{3.6}$$

with $D = \partial(\mathscr{E} + SP)\, u_i/\partial x_i + S/(\gamma - 1)\,\gamma/\sigma\,\partial^2\Theta/\partial x_1^2$ and $\mathscr{E} = \rho E$.

The splitting of the diffusive part into an explicit contribution and an implicit one in the x_2 direction is allowed by the large ratio of the mesh spaces in x_1 and x_2 directions.

The nonlinear diffusion terms have to be handled by an iterative method in order to overcome the very severe restriction on the time step which occurs in a explicit treatment.

3.2. *The Spectral Iterative Method with Finite Differences or Spectral Preconditioning*

Spectral Chebyshev approximations of such nonconstant or nonlinear operators lead to full, ill-conditioned, and asymmetric matrices. Direct application of implicit or/and iterative methods would require prohibitive computational resources. In order to overcome this difficulty, the use of iterative methods and preconditioning techniques within the framework of pseudo-spectral approximations has been suggested [11]. Since then, a number of iterative methods, with finite differences or finite elements preconditioning, have been suggested and tested on elliptic equations [19–23]. Among them, the minimal residual Richardson (MRR) method is the most useful and one of the most efficient, at least for simple boundary conditions like Dirichlet boundary conditions. Let us recall that the Richardson iterative method is the following. Let

$$L^*u = f, \tag{3.8}$$

be the equation to be solved, where L is the elliptic operator which comes out from the diffusion terms of the Eqs. (2.15)–(2.16), and f the right-hand side of Eqs. (3.5), (3.6). The iterative method is written as

$$u^{(n+1)} = u^{(n)} - \alpha L_{ap}^{-1}(L_{sp} u^{(n)} - f), \tag{3.9}$$

where L_{sp} is the Chebyshev approximation of the operator L, L_{ap} is the preconditioning operator, and α is a parameter adjusted in order to maximize the rate of convergence. A better strategy has been proposed in Refs. [19–21], by redefining this parameter at each iteration in order to minimize the residue. Such a method is called the minimal residual Richardson method (MRR). One possible formulation of the MRR is the following. Let u^0 be the initial guess; the initial residue is computed by

$$r^0 = f - L_{sp} u^0, \qquad z^0 = L_{ap}^{-1} r^0 \tag{3.10}$$

and the iterative process is written as

$$u^{(k+1)} = u^{(k)} + \alpha^k z^k, \qquad \text{where } \alpha^k = (r^k, L_{sp} z^k)/(L_{sp} z^k, L_{sp} z^k) \tag{3.11}$$

$$r^{(k+1)} = r^{(k)} - \alpha^k L_{sp} z^k, \tag{3.12}$$

$$z^{(k+1)} = L_{ap}^{-1} r^{(k+1)}. \tag{3.13}$$

The previous stage, given by formulas (3.5)–(3.6), provides the intermediate value u^{**}, and we have now to solve the equation

$$L_{sp} u^{n+1} = 2[\rho(z) + \rho'(x, z, t)]\, u^{**}(x, z, t)/\Delta t, \tag{3.14}$$

where

$$L_{sp} = 2[\rho(z) + \rho'(x, z, t)]/\Delta t - \partial^2/\partial z^2. \tag{3.15}$$

The preconditioning operator L_{ap} must be a very close approximation of the operator L_{sp}. It is generally the tridiagonal finite differences approximation of the operator L, obtained by taking the nonuniform mesh into account. We have numerically computed the spectrum of the operator $L_{ap}^{-1} L_{sp}$ for the operator (3.15) with finite differences preconditioning. Results are given in Table I, for Dirichlet

TABLE I

Spectrum of the Operator $L_{ap}^{-1} L_{sp}$ for Dirichlet Boundary Conditions, where Δt Is the CFL Time Step

M	Z	$2/\Delta t$	Spectrum
17	1	$1.1E+4$	[1, 1.28]
33	1	$4.2E+4$	[1, 1.55]
65	1	$1.7E+5$	[1, 1.78]

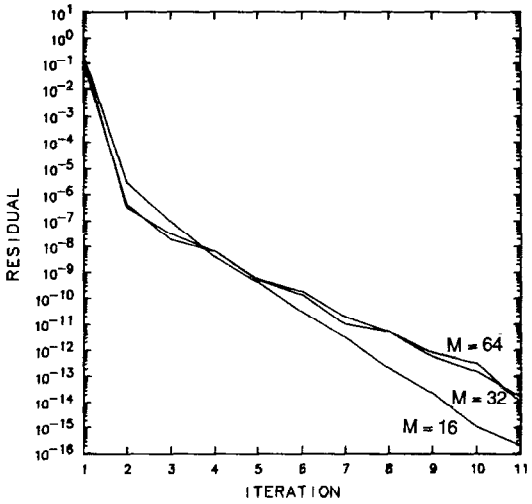

FIG. 1. Preconditioned residuals. Convergence history of the MRR with finite differences preconditioning for the operator defined in Eq. (3.14). The spatial resolutions are $M = 16$, 32, and 64 Chebyshev polynomials. The residue is given by Eq. (3.15) and it has been computed after the stage (3.12). Dirichlet boundary conditions have been used.

boundary conditions. The mean density varies from 1 to 2 and typical density fluctuations are given in Tables IV and V. For vanishing Δt^{-1}, we check that the spectrum becomes closer to the analytical value $[1, \pi^2/4]$ of the operator $L_{ap}^{-1} L_{sp}$ for $L = -\partial^2/\partial z^2$ [20].

In Fig. 1 we have displayed the history of the relative residue which is defined by

$$\text{Residue}^2 = \text{Max}((r, r)/(f, f)), \tag{3.16}$$

where f is the right-hand side of Eq. (3.14) and r is the residue given by (3.8). It appears that the behavior is roughly independent of the resolution M. The rate of convergence is dramatic at the beginning and decreases by almost one order of magnitude per iteration afterwards.

On the other hand, it has been pointed out [24], that on a vectorial computer, a

TABLE II

Spectrum of the Operator $L_{bp}^{-1} L_{sp}$ for Dirichlet Boundary Conditions, where Δt Is the CFL Time Step

M	Z	$2/\Delta t$	Spectrum
17	1	$1.4E+4$	[0.964, 1.042]
33	1	$5.6E+4$	[0.974, 1.051]
65	1	$2.3E+5$	[0.963, 1.065]

TABLE III

Spectrum of the Operator $L_{bp}^{-1}L_{sp}$ for Neumann Boundary Conditions, where Δt Is the CFL Time Step

M	Z	$2/\Delta t$	Spectrum
17	1	$1.9E+4$	[0.964, 1.042]
33	1	$7.5E+4$	[0.973, 1.051]
65	1	$3.0E+5$	[0.963, 1.065]

matrix multiplication can be faster, in terms of CPU time, than the inversion of a triadiagonal linear system executed in scalar mode. This suggestion leads to the following preconditioning

$$L_{bp} = 2\rho(z)/\Delta t - \partial^2/\partial z^2. \tag{3.17}$$

The Chebyshev approximation of the operator L_{bp} is a full matrix, but it does not depend on time and so, it needs to be inverted only once. It will be a close approximation to L_{sp} provided the relative density fluctuations are not too high. These behave as the square of the Mach number and Eq. (3.17) will be valid for low Mach number situations. The spectrum of the operator $L_{bp}^{-1}L_{sp}$ has been displayed in Tables II and III for the same mildly nonlinear solutions used in Table I, for different resolutions and boundary conditions.

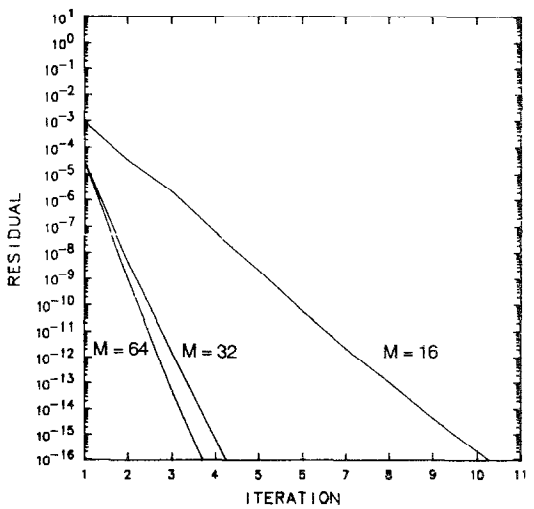

FIG. 2. Preconditioned residuals. Convergence history of the MRR with spectral preconditioning for the operator defined by Eq. (3.16). The spatial resolutions are $M = 16$, 32, and 64 Chebyshev polynomials. Dirichlet boundary conditions have been used.

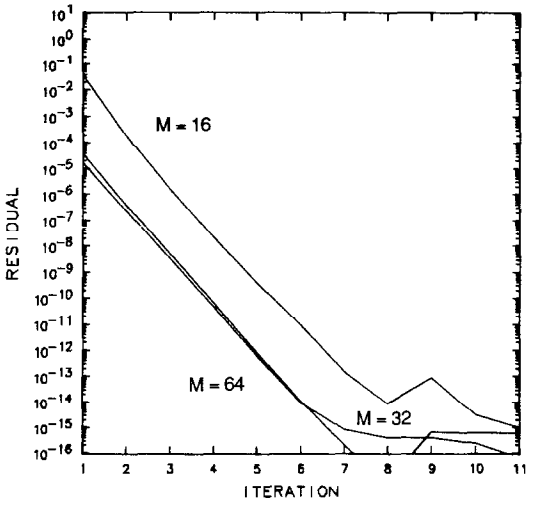

FIG. 3. Preconditioned residuals. Convergence history of the MRR with spectral preconditioning for the operator defined by Eq. (3.16). The spatial resolutions are $M = 16$, 32, and 64 Chebyshev polynomials. Neumann boundary conditions have been used.

These spectra are very close to unity and thus will lead to a high rate of convergence. The evolution of the residues with spectral preconditioning are presented in Fig. 2 and 3 for Dirichlet and Neumann boundary conditions. The efficiency increases with the resolution, especially between $M = 16$ and $M = 32$. However, we did notice that the convergence is slower with the Neumann boundary conditions. This point has been observed by several authors [24]. The spectral preconditioning defined by Eq. (3.17) is clearly more efficient than the finite differences preconditioning when compared in terms of the number of iterations needed to reach the spectral accuracy. Moreover, it takes less CPU time. In both cases boundary conditions are satisfied exactly.

4. PRELIMINARY RESULTS

4.1. *Validation of the Code*

The temporal numerical scheme and the weakness of the numerical diffusion of the code has been checked by computing the evolution of small disturbances very close to the threshold of the onset of convection. This critical Rayleigh number is known from the linear analysis around the conductive state [25]. Disturbances of the order of 10^{-10} at $0.97\, R_{crit}$ (resp. $1.03\, R_{crit}$) decay (resp. grow). In other words, the integration of the full nonlinear equations confirms the result of the linear theory and shows that, if some numerical diffusion is present, it does not perturb the transition to steady convection.

On the other hand, it is well known that, when an explicit scheme is used to solve an hyperbolic equation, the CFL stability condition is of the form

$$\Delta t < C\,\Delta z/(|V_{\max}| + C_s), \tag{4.1}$$

where Δz is the minimum mesh size, which occurs on the top and bottom boundaries in the vertical direction and C_s is the local sound speed. C is a constant equal to 1.4 for the second-order Adams–Bashforth predictor and third-order Adams–Bashforth corrector numerical scheme. We have checked that our code obeys this restriction, at least for mildly nonlinear solutions.

4.2. *Results*

In this preliminary study, we limited ourselves to steady state solutions.

Results, for the Neumann boundary conditions for the velocity and for a weak stratification parameter, have been displayed on Table IV, where R is the Rayleigh number, and $R_{\text{crit}} = 483.33$. $V_{\max}$ is the maximum of the velocity

$$(u_1^2(x, z) + u_2^2(x, z))^{1/2}$$

over the two-dimensional domain. The same definition has been used for the Mach number. $\rho_{\max}$ is the maximum of the relative density fluctuations over the two-dimensional domain, defined by

$$\rho_{\max} = \text{Max}(\rho(x, z)/\rho(z)). \tag{4.2}$$

The same definition holds for $T_{\max}$ and $P_{\max}$. Using values of Table IV we check, as expected, that $\rho_{\max}$ grows linearly as the square of the Mach number for Mach numbers smaller than 0.20.

The Nusselt number, which measures the efficiency of the convection has been computed by the following formula [8]:

$$Nu = (F_t - F_a)/(F_c - F_a). \tag{4.3}$$

TABLE IV

Rayleigh Number

	1933.32	1450.	1000.	800.	650.	570.33	551	531.67
R/R_{crit}	4	3	2.07	1.65	1.34	1.18	1.14	1.10
$V_{\max}$	29.900	22.603	15.112	11.181	7.656	5.479	4.835	4.127
Mach max.	0.221	0.203	0.175	0.152	0.122	0.094	0.084	0.073
Nu. bottom	2.804	2.455	1.997	1.708	1.428	1.245	1.143	1.195
$\rho_{\max}$	0.076	0.075	0.068	0.059	0.046	0.035	0.031	0.027
$T_{\max}$	0.086	0.075	0.063	0.052	0.041	−0.033	−0.030	−0.026
$P_{\max}$	0.073	0.062	0.050	0.039	0.028	0.020	0.017	0.014

This number is exactly zero in the conductive state and coincides with the classic definition in Boussinesq theory for vanishing values of the stratification of the parameter Z [8]. F_a and F_c are respectively the flux of the adiabatic gradient and the conductive flux. In natural variables they are

$$F_a = gK/C_p, \qquad F_c = K(T_l - T_u)/d. \tag{4.4}$$

The total flux is given by

$$F_t = K(Z + \langle \partial\Theta/\partial z \rangle), \tag{4.5}$$

where $\langle\ \rangle$ denotes the average value in a horizontal direction. In dimensionless variables the Nusselt number is written as

$$Nu = 1 + \langle \partial\Theta/\partial z \rangle / \{Z(m+1)(1/(m+1) - (\gamma - 1)/\gamma)\}, \tag{4.6}$$

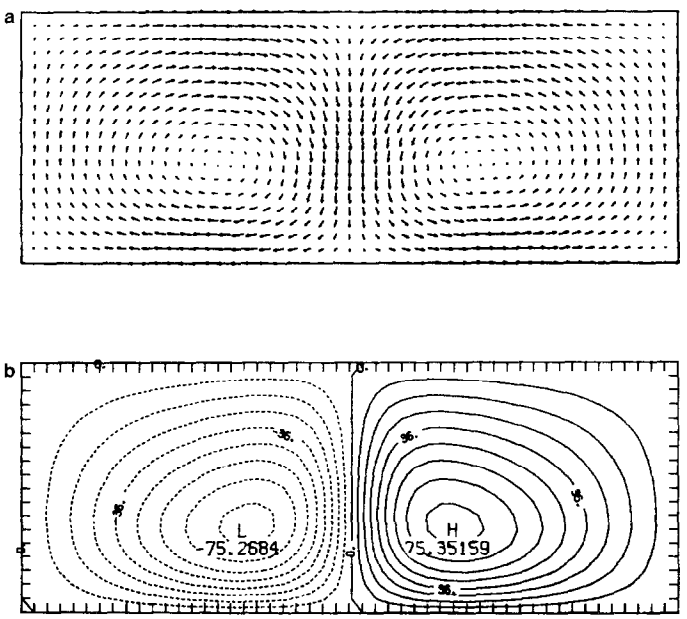

Fig. 4. Steady state solution for the Neumann boundary conditions for the velocity: (a) vector field, (b) vorticity, (c) relative density, (d) temperature, and (e) pressure fluctuations contours are, respectively, displayed. The Rayleigh number $R = 1000$ ($R = 2.07\ R_{crit}$). The stratification parameter $Z = 1$, the Prandtl number $\sigma = 0.71$, the aspect ratio $A = 2.79$, the polytropic index $m = 1$ and the ratio of specific heats $\gamma = 1.67$. Solid (broken) contours represent positive (negative) perturbations. More points have been used for the plot than for the simulation. Real values of the vorticity have been used. In Figs. 4c, d, and e, isovalues are scaled by a factor 10,000. The compressibility leads to a shift of the center of the rolls below and on the right (left) of the geometric center of the cell.

where

$$\langle \partial \Theta / \partial z \rangle(z) = 2 \sum_{j=0}^{M} a_{0j}\, dT_j(z)/dz, \tag{4.7}$$

and a_{ij} are the spectral coefficients of the temperature fluctuations. T_j is the Chebyshev polynomial of degree j. Because solutions are stationary, heat fluxes and then Nusselt numbers have to be equal at the top and the bottom of the layers. This provides a stopping criterion for the integration process which has been stopped when

$$(Nu_{\text{top}} - Nu_{\text{bot.}})/Nu_{\text{top}} < 10^{-4}$$

is satisfied.

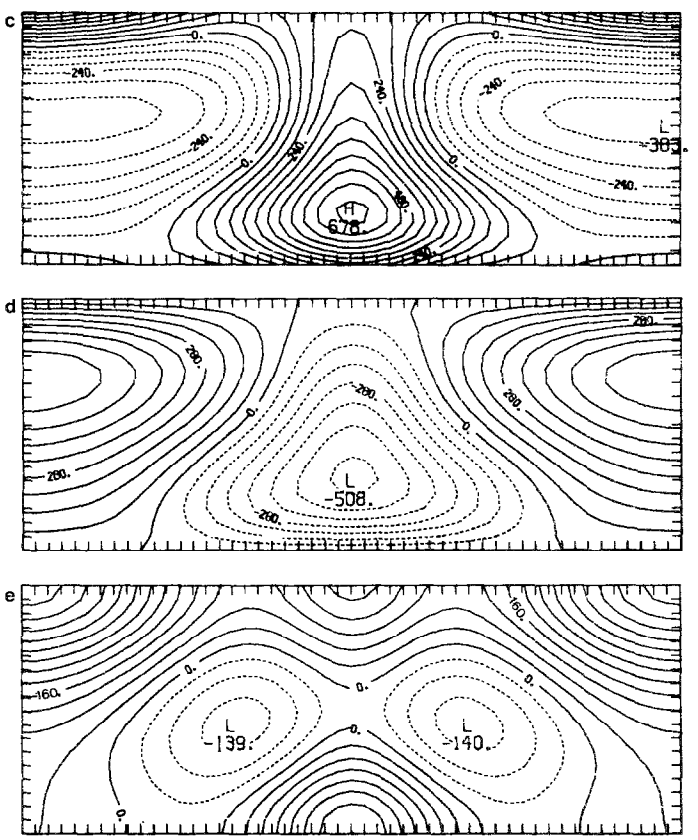

FIGURE 4 *(continued)*

The spatial resolution was 16×17 modes and we have checked that the highest coefficients of the expansion (3.1) were several orders of magnitude lower that the first ones.

In Figs. 4, we present the isovalues of the vorticity, the relative density, the temperature, and the pressure fluctuations for a steady state with Neumann boundary conditions for the velocity. Since the value of the stratification parameter is $Z = 1$, the ratios of the density, temperature, and pressure between the top and the bottom are 2, 2, and 4, respectively, the polytropic index being equal to 1. Recall that the only nonzero component of the vorticity ω is given by

$$\omega_y(x, z, t) = \partial u_2(x, z, t)/\partial x - \partial u_1(x, z, t)/\partial z. \tag{4.8}$$

As it is now well known, rolls of convection are deformed by the compressibility [5, 8, 10]. The strongest density fluctuations occur in the lower part of the central downward plume where the temperature fluctuations are lowest. As it is detailed

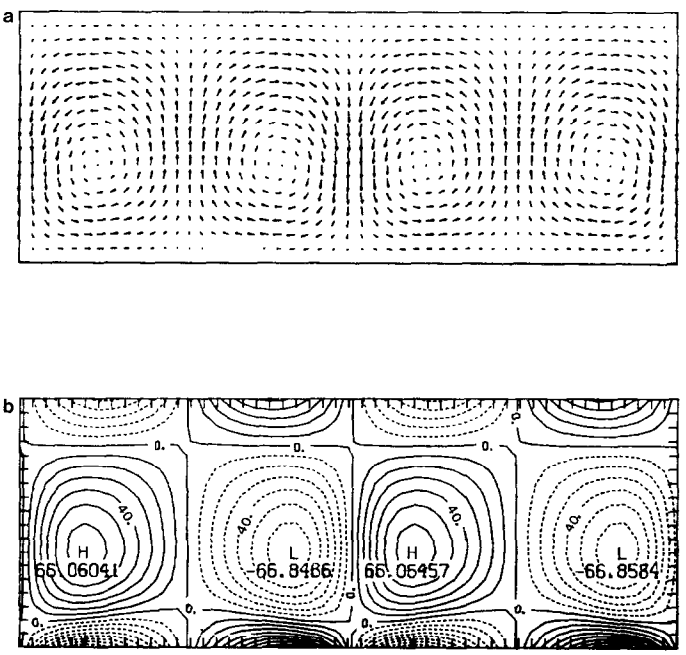

FIG. 5. Steady state solution for the Dirichlet boundary conditions for the velocity: (a) vector field, (b) vorticity, (c) relative density, (d) temperature, and (e) pressure fluctuations contours are respectively displayed. The Rayleigh number $R = 2000$. The stratification parameter $Z = 2$, the Prandtl number $\sigma = 0.71$, the aspect ratio $A = 2.79$, the polytropic index $m = 1$, and the ratio of specific heats $\gamma = 1.67$. Rolls of the quarter of the spatial period and boundary layer appear on these patterns.

TABLE V

Rayleigh number	V_{max}	Mach max.	Nu. bottom	ρ_{max}	T_{max}	P_{max}
2000	8.775	0.115	1.555	0.060	0.063	0.059

in Ref. [26], the pressure is responsible for the change in direction of the flow. Consequently, the largest pressure fluctuations must arise where the flow diverges.

In Figs. 5 and in Table V, we have displayed an example of a solution with Dirichlet boundary conditions for the velocity. The value of the stratification parameter Z is now equal to 2, and the ratios of the density temperature, and pressure between the top and the bottom are 3, 3, and 9, respectively, with the polytropic index still equal to unity. The solution for this type of boundary con-

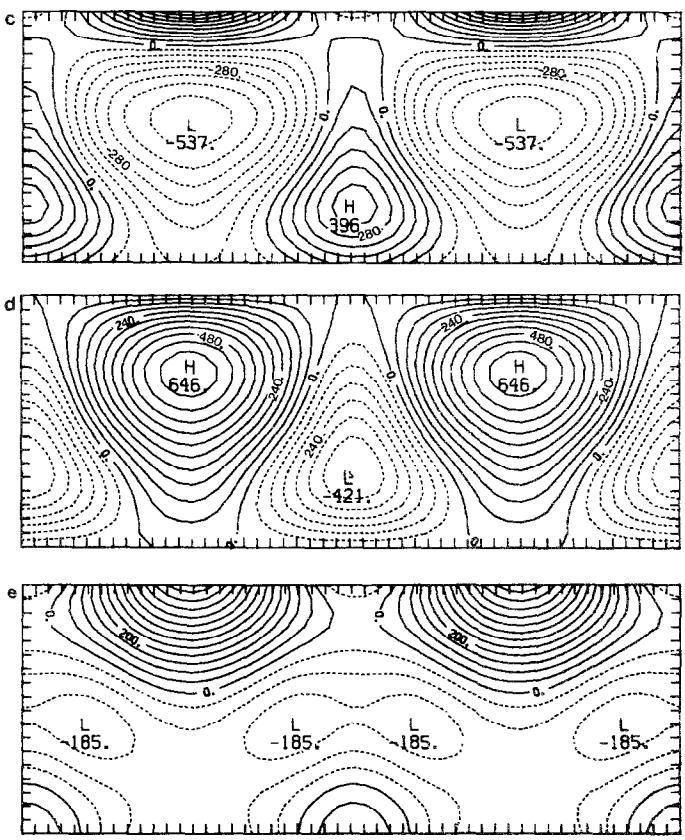

FIGURE 5 *(continued)*

ditions is formed by four rolls. The periodicity is now half the aspect ratio. Spatial patterns of Figs. 5 exhibit clearly the boundary layer of the flow on the top and bottom boundaries.

4.3. *Variation of the Nusselt Number and the Maximum Velocity as Functions of the Rayleigh Number*

As in static critical phenomena, it is possible to compute critical exponents close to the transition. The interest of such coefficients results from the observation that the values of the critical exponents are rather insentive to the details of the system. In other words, such coefficients are, at least for a class of systems, universal [27].

In the incompressible case, the critical exponent of the Nussel number and the maximum velocity are known both from experiments and numerical simulations. From Ref. [28], we can write

$$(Nu-1)\,R \sim (R-R_{\text{crit}})^{\alpha} \tag{4.9}$$

$$V_{\max} \sim (R-R_{\text{crit}})^{\beta} \tag{4.10}$$

with $\alpha = 1$ and $\beta = \frac{1}{2}$, for the incompressible case. These relations hold very close to the transition for Rayleigh numbers such that

$$(R-R_{\text{crit}})/R_{\text{crit}} < \varepsilon^{*}. \tag{4.11}$$

Following Ref. [28], $\varepsilon^{*} \sim 6$.

We have plotted relations (4.9)–(4.10) in Figs. 6 and 7 with the straight line of

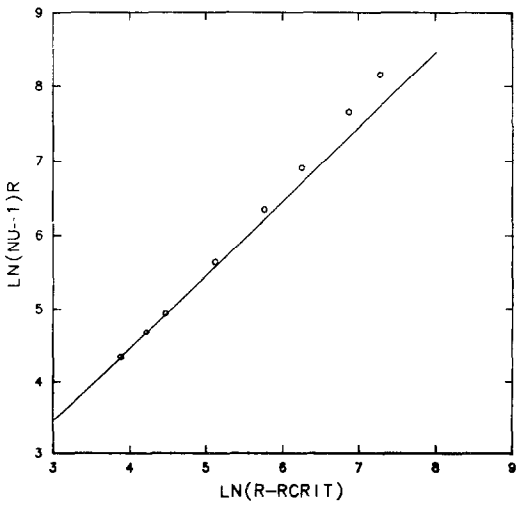

FIG. 6. Variation of $\text{Ln}(Nu-1)\,R$ with $\text{Ln}(R_{\text{crit}}-R)$; Neumann boundary conditions for the velocity. The stratification parameter is equal to 1: (○) numerical value; — straight line of slope 1.

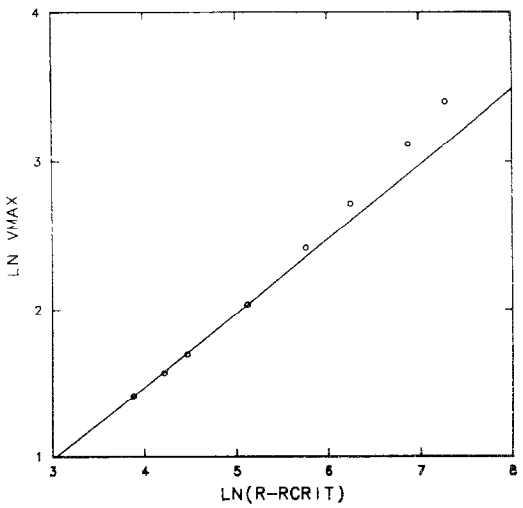

FIG. 7. Variation of Ln V_{max} with $\mathrm{Ln}(R_{crit} - R)$: same conditions as in Fig. 6: — straight line of slope $\frac{1}{2}$.

slopes 1 and $\frac{1}{2}$. It appears that these power laws hold for the weakly compressible case, for $\varepsilon^* < 0.35$. We have computed the slope of both straight lines by the least squares method, using the first three or four points. The results are

$$\begin{aligned} &\alpha = 1.027 \quad \beta = 0.481 \quad \text{for three points,} \\ &\alpha = 1.047 \quad \beta = 0.501 \quad \text{for four points,} \end{aligned} \tag{4.12}$$

which are reasonable approximations of the values $\alpha = 1$ and $\beta = \frac{1}{2}$. We guess that these critical exponents hold for any value of the stratification parameter Z with the restriction that the larger the Z parameter, the smaller the range of ε^*. Measurements of the critical exponents and steady state solutions displayed exhibit the classic symmetry with respect to the middle of the cell. It confirms the accuracy of the temporal numerical scheme of the pseudo-spectral code, since any spatial resolution or any truncated model of convection yields the good critical exponents [28].

5. CONCLUSION

We have developed a numerical algorithm for the solution of two-dimensional fully compressible thermal convection. The fluid is a perfect gas with constant dynamic viscosity and thermal conductivity. The algorithm uses finite differences in time and spatial truncated series of Fourier functions in the horizontal direction and Chebyshev polynomials in the inhomogeneous direction. Convective and

pressure terms are handled by a second-order Adams–Bashforth predictor and a third-order Adams–Bashforth corrector. Nonlinear diffusion terms are treated by an efficient iterative method with spectral preconditioning. Both Neumann and Dirichlet boundary conditions for the velocity have been developed. The critical exponents defined near the transition have been found to be the same as in the incompressible case, but hold for a smaller range. This shows, as in Ref. [29], that spectral methods which have been used successfully in incompressible fluids can be extended to the full Navier–Stokes equations. However, the high frequency acoustic waves impose a very severe restriction on the time step. Time-dependent solutions have also been found and will be analyzed in a forthcoming paper.

ACKNOWLEDGMENTS

The major part of this work has been done while the author was at the Center for Nonlinear Studies at the Los Alamos National Laboratory under the French Grant DRET 85.34.819.00.470.75.01. All numerical computations have been carried out at LANL. I would like to thank Drs. C. S. Tan, J. M. Hyman, G. D. Doolen, M. M. Doria, J. K. Dukowicz, G. A. Glatzmaier, I. G. Kevrekidis, C. McKinstrie, J. Leorat, P. S. Lomdahl, T. Manteuffel, A. Meurant, Y. Morchoisne, B. Nicholaenko, S. A. Orszag, Y. Pomeau, B. Scheurer, E. A. Spiegel, and K. H. Winkler for several discussions and suggestions along this work. I am indebted to C. S. Tan for providing FORTRAN routines about the collocation approximation of differential operators. I am very grateful to the staff of the Center for Nonlinear Studies at the Los Alamos National Laboratory for their kind hospitality. Eigenvalues were obtained by the EISPACK routines and graphics by the NCAR package.

REFERENCES

1. R. G. VOIGT, D. GOTTLIEB, AND M. Y. HUSSIANI, in *Proceedings Symposium on Spectral Methods for PDE* (Soc. Indus. Appl. Math., Philadelphia, 1984).
2. D. GOTTLIEB AND S. A. ORSZAG, in *Numerical Analysis of Spectral Methods: Theory and Applications*. CBMS-NSF Regional Conferences Series in Applied Mathematics, (Soc. Indus. Appl. Math., Philadelphia, 1977).
3. D. D. SCHNACK, D. C. BAXTER, AND E. J. CARAMANA, *J. Comput. Phys.* **55**, 485 (1984).
4. J. LATOUR, E. A. SPIEGEL, J. TOOMRE, AND J. P. ZAHN, *Astrophys. J.* **207**, 233 (1976).
5. J. M. MASSAGUER AND J. P. ZAHN, *Astro. Astrophys.* **87**, 315 (1980).
6. G. A. GLATZMAIER, *J. Comput. Phys.* **55**, 461 (1984).
7. D. O. GOUGH, *J. Atmosph. Sci.* **26**, 448 (1976).
8. E. GRAHAM, *J. Fluid Mech.* **70**, 689, (1975). E. GRAHAM, in *IAU Colloquium 38, Problems of Stellar Convection, 1977*, edited by E. A. Spiegel and J. P. Zahn (Springer-Verlag, Berlin, 1977).
9. K. L. CHAN AND C. L. WOLFF, *Astrophys. J.* **263**, 935 (1982).
10. N. E. HURLBURT, J. TOOMRE, AND J. MASSAGUER, *Astrophys. J.* **282**, 557 (1984).
11. S. A. ORSZAG, *J. Comput. Phys.* **37** 70 (1980).
12. E. A. SPIEGEL, *Astrophys. J.* **141**, 1068 (1965).
13. S. A. ORSZAG AND L. C. KELLS, *J. Fluid Mech.* **96**, 159 (1980).
14. P. L. SULEM, C. SULEM, AND O. THUAL, "Direct Numerical Simulation of Three-Dimensional Convection in Liquids Metal," Fourth Beer Sheva Seminar on Magnetohydrodynamic Flows and Turbulence, Ben Gurion University of the Negev, Beer Sheva, Israel, February 27–March 2, 1984.
15. P. LE QUERE AND T. ALZIARY DE ROQUEFORT, *J. Comput. Phys.* **57**, 210 (1985).

16. S. A. ORSZAG AND J. B. MCLAUGHLIN, *J. Fluid Mech.* **122**, 123 (1982).
17. L. F. SHAMPINE AND M. K. GORDON, *Computer Solution of Ordinary Differential Equations* (Freeman, San Francisco, 1975).
18. B. WENDROFF, *Theoretical Numerical Analysis* (Academic Press, New York, 1966).
19. T. A. ZANG, Y. S. WONG, AND M. Y. HUSSIANI, *J. Comput. Phys.* **48**, 485 (1982).
20. P. HALDENWANG, G. LABROSSE, S. ABBOUDI, AND M. DEVILLE, *J. Comput. Phys.* **55**, 115 (1984).
21. C. S. TAN, *J. Comput. Phys.* **59**, 81 (1985).
22. C. CANUTO AND A. QUARTERONI, *J. Comput. Phys.* **60**, 315 (1985).
23. M. DEVILLE AND E. MUND, *J. Comput. Phys.* **60**, 517 (1985).
24. C. S. TAN, Department of Aeronautics and Astronautics, Massachusetts Institute of Technology, Cambridge, MA, private communication, (1986).
25. D. O. GOUGH, D. R. MOORE, E. A. SPIEGEL, AND N. O. WEISS, *Astrophys. J.* **206**, 536 (1976).
26. J. P. ZAHN, in *Stellar Turbulence*, Lecture Notes in Physics Vol. 114, edited by D. F. Gray and J. L. Linsky, (Springer Verlag, Berlin, 1979), p. 1.
27. O. G. MOURITSEN, *Computer Studies of Phase Transitions and Critical Phenomena* (Springer Verlag, Berlin, 1984).
28. J. K. PLATTEN AND J. C. LEGROS, *Convection in Liquids* (Springer Verlag, Berlin, 1984).
29. G. ERLEBACHER AND M. Y. HUSSAINI, "Incipient Transition Phenomena in Compressible Flows over a Flat Plate," ICASE Report 86–39, NASA Langley R. C., June 1986; in *Proceedings, 10th Int. Conference on Numerical Methods in Fluid Dynamics, Beijing, China.*